Turk J Elec Engin, VOL.15, NO.1 2007, © TÜBİTAK

Analysis of Finline Structures with Consideration of Metallization Thickness and Substrate Mounting Grooves

Abderrahmane OUADI[1], **Hadj BOURDOUCEN**[2]
[1] *University of Mohammed Bouguerra, Department of Electrical Engineering, Boumerdes, 35000, ALGERIA*
[2] *Sultan Qaboos University, College of Engineering, Department of Electrical and Computer Engineering, P O Box 33, Al Khodh, Muscat 123, OMAN*
e-mail: hadj@squ.edu.om

Abstract

In this paper, mathematical analysis and numerical calculations of main parameters of finline structures with finite metallization thickness and substrate mounting grooves are developed based on the Method of Lines (MoL). The results obtained provide confirmation of the validity of the technique used and prove its simplicity and adequacy for treating different types of planar structures mainly finline based structures.

Unilateral and bilateral finlines including practical parameters, such as metallization thickness and grooves' depths, have been investigated. The effect of these two parameters have been discussed based on realistic configurations and the results show that, at higher frequencies, the grooves supporting the substrate cannot be neglected and, in addition, their influence is more significant than the effect of finite thickness metallic strips. The isolated finline with more complex configuration with a particular interest in applications involving active components was also analyzed. The obtained results confirm the previous published predictions for these types of structures.

1. Introduction

The preferred transmission line for millimeter wave integrated circuits is known as the one which avoids miniaturization and yet offers potential for low-cost production through different batch processing techniques. Many practical transmission lines are proposed to overcome the common transmission lines liability and associated problems that appear at higher frequencies. In this regard, Shneider has proposed what is known as suspended substrate microstrip lines [1] and Meier, the finlines [2].

With growing interest of components and systems designs, there has been increasing activity concerning theoretical foundations of these structures. During the past several years, divers papers have been published [3-4,6-11] using various numerical techniques to determine the propagation characteristics of finline structures. However, most of the works published did not take into account the real effect of finite thickness of metallization strips and supporting grooves.

The metallization thickness has been taken into account by Beyer [8] and Vahldieck [9] using the mode-matching method and by Kitazawa [10] using the network analytical method and also by R. Mansour

et. al. employing the conservation of complex power technique [11]. The effects of side wall grooves, which have been employed in a real realization of finlines or generally used in E-plane circuits that support the substrate mechanically, has been considered as well in references [9-11]. The effect of metal strip thickness on propagation characteristics of multiconductor planar transmission line structures has been taken into consideration by Saad and Schunemann [5], in which the approximation involved is only valid for structures with large slot widths. A more accurate analysis has been presented in [12-15].

In the present analysis, hybrid-mode approach is used to determine the effective dielectric constant for dominant and higher modes as well as the characteristic impedance for special unilateral finline structure. The analysis can also be applied to a wide variety of planar and quasi-planar transmission line structures with multiconductors and multilayer isotropic/anisotropic substrates.

Besides the versatility and the flexibility of the approach presented in this paper in treating complicated structures such as the one in [19-20], it is numerically efficient and includes practical considerations such as metallization thickness and substrate mounting grooves. In addition to this, another important parameter disregarded by overall published analysis has to be taken into consideration. This is particularly important for quasi-planar E-printed transmission line structures which do not support TEM-wave propagation, as in the case of the finline structures which have to be either isolated from the metallic housing at dc, or directly connected to the waveguide housing.

2. Formulation of the Problem

To present the analysis adopted, a realistic finline structure of interest, which has been used by Meier [2] as shown in Figure 1 has been considered. The cross section of this practical structure is represented in Figure 2. This integrated finline structure was developed to operate at millimeter wavelengths where its cross section is suitable for mounting semiconductor devices.

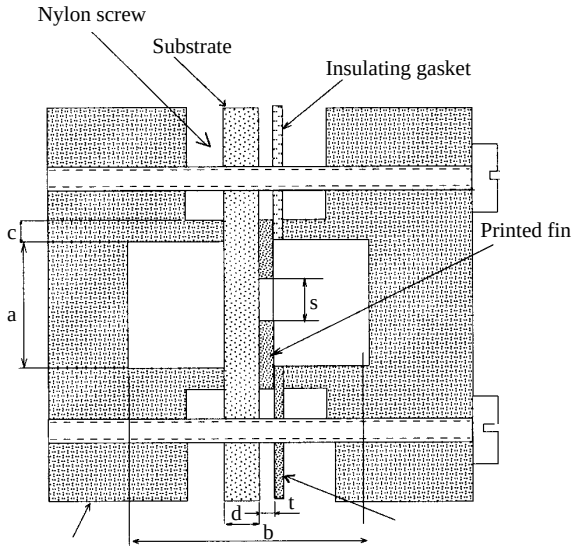

Figure 1. Real unilateral finline structure and illustration of its fixation.

In this structure of Figure 1, the upper fin is insulated from the housing at dc by a dielectric gasket, where, according to Meier [2], it is grounded at RF by choosing the thickness of the broad walls to be a quarter wavelength in the dielectric medium. However, the lower fin is grounded directly by a metal gasket

to provide a dc return in case of solid-state applications. It is important to note that the typical realistic structure presented in Figure 1 may have symmetrical as well as unsymmetrical fins.

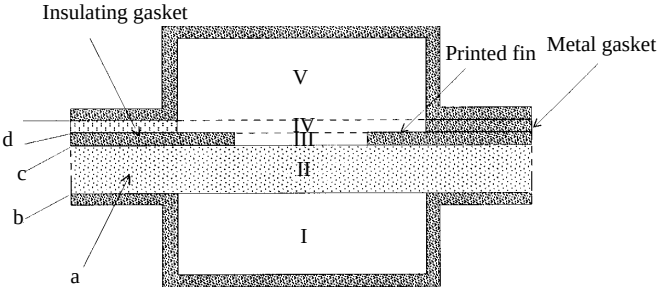

Figure 2. Unilateral finline structure with mounting grooves and with a gasket insulator.

For the analysis of the structure shown in Figure 2, it is worth noting that the regions I, II, III and V are homogeneous isotropic or anisotropic dielectric layers, where in each region the wave equations have to be solved. The tangential field relationships needed for the matching need to be satisfied and have been presented elsewhere [21]. However, the treatment of inhomogeneous layers, such as region IV, has not yet been addressed before and therefore, is presented in the following sections.

2.1. Description of discretization scheme for inhomogeneous dielectric

The homogeneous layer consists of an abrupt transition of two or more dielectric regions aligned in the same layer. In order to analyze microwave structures formed by homogeneous and inhomogeneous dielectric layers, the problem of inhomogeneous layer should be solved first, and the resulted analysis must be mixed with that of homogeneous layers. For this purpose, an inhomogeneous layer which consists of two dielectric abrupt transitions as illustrated in Figure 3 has been considered. It can be noted that the dielectric constant of each region is function of x. In this way, the problem of more than two transitions can be generalized without difficulty.

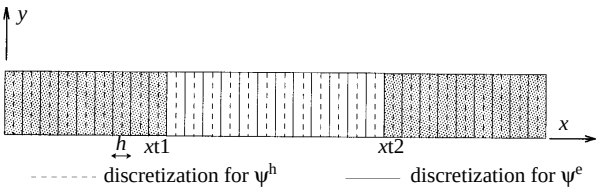

Figure 3. Uniform discretization of homogeneous dielectric layer.

Following Collin [16-18] the wave field in this inhomogeneous layer can be determined from two vector potentials and, which have only one component in the dielectric of transition, namely the x- direction. The electromagnetic field is related to these potentials as per the following expressions:

$$E = \varepsilon_r(x)^{-1}\nabla \times \nabla \times \pi_e - jk_o\nabla \times \pi_h \tag{1a}$$

$$\eta_o H = jk_o\nabla \times \pi_e + \nabla \times \nabla \times \pi_h \tag{1b}$$

with $k_o = \omega\sqrt{\varepsilon_o\mu_o}$ and $\eta_o = \sqrt{\mu_o/\varepsilon_o}$. The vectors of potentials π_e and π_h, which are x-directed (unit $\hat{a}_x$) and propagating over a cross-section of waveguiding structure along the z-direction, may be written as

$$\pi_e(x,y) = \psi^e(x,y)e^{-jk_z z}k_o^{-2}\hat{a}_x \tag{2a}$$

$$\pi_h(x,y) = \psi^{\,h}(x,y)e^{-jk_z z}k_o^{-2}\hat{a}_x \tag{2b}$$

The potential functions ψ^e and ψ^h must fulfil the Helmotz equation (3a) and the Sturm-Liouville differential equation (3b) respectively:

$$\frac{\partial^{\,2}\psi^{\,h}}{\partial x^2} + \frac{\partial^{\,2}\psi^{\,h}}{\partial x^2} + \left(\varepsilon_r(x)k_o^2 - k_z^2\right)\psi^{\,h} = 0 \tag{3a}$$

$$\varepsilon_r(x)\frac{\partial}{\partial x}\left(\frac{1}{\varepsilon_r(x)}\frac{\partial\psi^{\,e}}{\partial x}\right) + \frac{\partial^{\,2}\psi^{\,e}}{\partial x^2} + \left(\varepsilon_r(x)k_o^2 - k_z^2\right)\psi^{\,e} = 0 \tag{3b}$$

This is in association with the following boundary conditions on electric and magnetic walls.

Electric walls:

$$\psi^{\,h} = 0 \quad ; \quad \frac{\partial\psi^{\,e}}{\partial x} = 0 \tag{4a}$$

Magnetic walls:

$$\psi^{\,e} = 0 \quad ; \quad \frac{\partial\psi^{\,h}}{\partial x} = 0 \tag{4b}$$

In order to solve the partial differential equations (PDE) (3) using the well known Method of Lines [18], both the potentials and dielectric constant need to be discretized with respect to the x-variable. Two line systems are used for the full-wave analysis so that the lateral boundary conditions of the potentials are satisfied, as shown in Figure 3 for a uniform discretization scheme. Two different discretized dielectric constants are then obtained for each potential function as,

$$\text{for } \psi^{\,e} : \varepsilon_r(x) \longrightarrow diag(\varepsilon_r(x_e) = \varepsilon_e \tag{5a}$$

$$\text{for } \psi^{\,h} : \varepsilon_r(x) \longrightarrow diag(\varepsilon_r(x_h) = \varepsilon_h \tag{5b}$$

In general, the values of ε_h at the discretization lines x_t (transition) positioned at the interfaces where the dielectric constant changes abruptly, one must take into account, as indicated in [17,18], special considerations such as $\varepsilon_r(x_t) = \left(\varepsilon_r(x_t^+) - \varepsilon_r(x_t^-)\right)/2$. Therefore, the first and second differential operators with respect to x-direction can be approximated by finite difference approximation, and may be written as follows

$$h\frac{\partial\psi^{\,h}}{\partial x} \longrightarrow D\psi^h \tag{6a}$$

$$h\frac{\partial\psi^{\,e}}{\partial x} \longrightarrow -D^t\psi^e \tag{6b}$$

$$h^2\frac{\partial^{\,2}\psi^{\,h}}{\partial x^2} \longrightarrow -D^tD\psi^{\,h} = -P_h^{\varepsilon}\psi^{\,h} \tag{6c}$$

$$h^2\varepsilon_r(x)\frac{\partial}{\partial x}\left(\frac{1}{\varepsilon_r(x)}\frac{\partial\psi^{\,e}}{\partial x}\right) \longrightarrow -\varepsilon_e D\varepsilon_h^{-1}D^t\psi^{\,h} = -P_e^{\varepsilon}\psi^{\,e} \tag{6d}$$

where ψ^e and ψ^h are column vectors of the discretized potentials, and D is the difference operator which depends on the lateral boundaries. The two PDEs (3) can now be written in a unified form as:

$$\left\{-h^{-2}P^{\varepsilon} + k_o^2\varepsilon + \left(\frac{d^2}{dy^2} - k_z^2\right)\right\}\Psi = 0 \tag{7}$$

Where to the matrix quantities P^{ε}, ε and the vector potential function Ψ, have to be added either a subscript e or h.

In order to decouple the system (7), it is necessary to perform a suitable transformation as:

$$\Psi = R\tilde{\Psi} \tag{8}$$

where $\tilde{\Psi}$ is the transformed column vector of the discretized potential functions, and S the transformation matrix, (with $R = T.S$ as pointed out in 11-a and 11-b below), that is obtained from the following eigenvalue problem:

$$\left(\, h^{-2}k_o^{-2}P^{\varepsilon} - \varepsilon \,\right) R = R\lambda \tag{9}$$

where λ is a diagonal matrix of distinct eigenvalues. To solve eq. (9), it is necessary to replace P^{ε} by its corresponding values P_e^{ε} and P_h^{ε}. This leads to λ_e, λ_h and S_e, S_h. The eigenvalue problem becomes

$$\left(\, h^{-2}k_o^{-2}\varepsilon_e D\varepsilon_h^{-1}D^t - \varepsilon_e \,\right) R_e = R_e\lambda_e \tag{10a}$$

$$\left(h^{-2}k_o^{-2}D^tD - \varepsilon_h \,\right) R_h = R_h\lambda_h \tag{10b}$$

However, it is possible to split each of the transformations S_e and S_h into two independent transformations. Indeed, let

$$R_e = T_eS_e \tag{11a}$$

$$R_h = T_hR_h \tag{11b}$$

Then eq. (10) becomes

$$Q_eS_e = S_e\tilde{\lambda} \tag{12a}$$

$$Q_hS_h = S_h\tilde{\lambda}_h \tag{12b}$$

and

$$Q_e = \bar{\varepsilon}_e\,\bar{\delta}\,\varepsilon_h^{-1}\,\bar{\delta}^{\,t} - \bar{\varepsilon}_e \tag{13a}$$

$$Q_h = \bar{\lambda}_h^2 - \bar{\varepsilon}_h \tag{13b}$$

where $\bar{\delta} = (k_oh)^{-1}\,\delta$; $\delta = T_e^tDT_e$; $\bar{\lambda}_h^2 = \bar{\delta}^{\,t}\bar{\delta}$; $\bar{\varepsilon}_e = T_e^t\varepsilon_eT_e$; $\bar{\varepsilon}_h = T_h^t\varepsilon_hT_h$.

The transformation matrices T_e and T_h are the matrices used for homogeneous layers and S_e and S_h are supplementary matrices to account for the inhomogeneous dielectric slab layers. Solving the

eigenvalue problems of eq. (12), the diagonal matrices $\tilde{\lambda}_e$ and $\tilde{\lambda}_h$ of real and distinct eigenvalues, and the transformations matrices S_e and S_h are also derived numerically.

The yielded system of uncoupled ODEs for $\tilde{\Psi}_e$ and $\tilde{\Psi}_h$ then becomes,

$$\left(I \frac{1}{k_o^2} \frac{d^2}{dy^2} \; - \; k_z^2 \right) \; \tilde{\Psi}_{e,h} = 0 \tag{14}$$

where $ky_{e,h}(y) = diag\,(kyie, h/k_o)$, with $ky_{ie,h} = \left(\tilde{\lambda}_{ie,h} + \varepsilon_{re} \right) k_o^2$.

The general solution of eq. (14) for the i-th component of $\tilde{\Psi}_{e,h}$ is given by

$$\tilde{\Psi}_i(y) = A_{ie,h} \cos\left(ky_{ie,h}\; y\right) + B_{ie,h} \sin\left(ky_{ie,h}\; y\right) \tag{15}$$

The elimination of the constants $A_{ie,h}$ and $B_{ie,h}$ leads to the following solution for an arbitrary layer with thickness d, where A and B are its bottom and top interfaces where

$$\begin{bmatrix} \frac{d}{dy}\tilde{\Psi}_A \\ \frac{d}{dy}\tilde{\Psi}_B \end{bmatrix} \; = \; k_o k_{y^v}^2 \begin{bmatrix} \gamma & \alpha \\ \alpha & \gamma \end{bmatrix} \begin{bmatrix} -\tilde{\Psi}_A \\ \tilde{\Psi}_B \end{bmatrix} \tag{16}$$

$$\alpha = diag\left(\frac{ky_i}{k_o} \sinh\left(ky_i\; d\right) \right)^{-1}, \quad \gamma = diag\left(\frac{ky_i}{k_o} \tanh\left(ky_i\; d\right) \right)^{-1}, \quad k_{yv} = diag\left(\frac{k_{y_i^v}}{k_o} \right) \tag{17}$$

Note that in eq. (16), the superscript γ needs to to be substituted by either e or h to denote the corresponding potential vector.

2.2. Calculations for the field components

The electromagnetic field components are calculated from the potentials ψ^e and ψ^h according to eqs. (1) and (2). After discretization and transformation of the fields T_e and T_h, and approximating the derivatives with respect to x variable by a differential operator, one can get the transformed field components necessary for the matching on the interfaces as

$$\bar{E}_x = -\bar{\varepsilon}_e^{-1} Q_e S_e \tilde{\Psi}_e \tag{18}$$

$$\eta_o \bar{H}_x = -Q_h S_h \tilde{\Psi}_h \tag{19}$$

$$j\bar{E}_z = -\frac{1}{k_o} S_h \frac{d}{dy} \tilde{\Psi}_h - \varepsilon_h^{-1}\, \tilde{\delta}^t S_e \tilde{\Psi}_e \tag{20}$$

$$j\eta_o \bar{H}_z = -\frac{1}{k_o} S_e \frac{d}{dy} \tilde{\Psi}_e + \tilde{\delta}\; S_h\; \tilde{\Psi}_h \tag{21}$$

with $\tilde{\delta} = \sqrt{\varepsilon_{re}}\bar{\delta}$

Whereas for y- field component, necessary for power computation, is given by the following expressions

$$\bar{E}_y = -\bar{\varepsilon}_h^{-1}\, \bar{\delta}^t\, S_e \left(\frac{1}{k_o} \frac{d}{dy} \tilde{\Psi}_e \right) - \sqrt{\varepsilon_{re}}\; S_h\; \tilde{\Psi}_h \tag{22}$$

$$\eta_o \bar{H}_y = \bar{\delta}\ S_h\ \left(\frac{1}{k_o}\frac{d}{dy}\tilde{\Psi}_e \right) + \sqrt{\varepsilon_{re}}\ S_e\ \tilde{\Psi}_e \tag{23}$$

The corresponding transformation of the fields are performed by the following equalities:

$$E_y = T_h\ \bar{E}_y \quad ; \quad E_z = T_h\ \bar{E}_z \quad ; \quad H_x = T_h\ \bar{H}_x$$

$$E_x = T_e\ \bar{E}_x \quad ; \quad H_y = T_e\ \bar{H}_y \quad ; \quad H_z = T_e\ \bar{H}_z \tag{24}$$

The set of equations (15)-(21) have to be used for both interfaces A and B and when substituting $\frac{1}{k_o}\frac{d}{dy}\tilde{\Psi}$ by means of (16), one can get:

$$\begin{bmatrix} \bar{E}_{xA} \\ \bar{E}_{xB} \end{bmatrix} = -\bar{\varepsilon}_e^{-1} Q_e S_e \begin{bmatrix} \tilde{\Psi}_{eA} \\ \tilde{\Psi}_{eA} \end{bmatrix} = -\left(\bar{\delta}\ \bar{\varepsilon}_h^{-1}\ \bar{\delta}^{\,t} - I_e\right)\ S_e \begin{bmatrix} \tilde{\Psi}_{eA} \\ \tilde{\Psi}_{eA} \end{bmatrix} \tag{25}$$

$$\eta_o \begin{bmatrix} \bar{H}_{xA} \\ \bar{H}_{xB} \end{bmatrix} = -Q_h S_h \begin{bmatrix} \tilde{\Psi}_{hA} \\ \tilde{\Psi}_{hA} \end{bmatrix} = -\left(\bar{\lambda}_h - \bar{\varepsilon}_{\,h}\right)\ S_h \begin{bmatrix} \tilde{\Psi}_{hA} \\ \tilde{\Psi}_{hA} \end{bmatrix} \tag{26}$$

$$\begin{bmatrix} j\bar{E}_{zA} \\ j\bar{E}_{zB} \end{bmatrix} = -S_h k y_h^2 \begin{bmatrix} -\gamma_h & \alpha_h \\ -\alpha_h & \gamma_h \end{bmatrix} \begin{bmatrix} \tilde{\Psi}_{hA} \\ \tilde{\Psi}_{hA} \end{bmatrix} - \bar{\varepsilon}_h^{-1}\,\tilde{\delta}^{\,t} S_e \begin{bmatrix} \tilde{\Psi}_{eA} \\ \tilde{\Psi}_{eA} \end{bmatrix} \tag{27}$$

$$\eta_o \begin{bmatrix} j\bar{H}_{zA} \\ j\bar{H}_{zB} \end{bmatrix} = -S_e k y_e^2 \begin{bmatrix} c-\gamma_e & \alpha_e \\ -\alpha_e & \gamma_e \end{bmatrix} \begin{bmatrix} \tilde{\Psi}_{eA} \\ \tilde{\Psi}_{eA} \end{bmatrix} + \tilde{\delta}\ S_h \begin{bmatrix} \tilde{\Psi}_{hA} \\ \tilde{\Psi}_{hA} \end{bmatrix} \tag{28}$$

Whereas the field components in the y-direction are given by:

$$\begin{bmatrix} \bar{E}_{yA} \\ \bar{E}_{yB} \end{bmatrix} = -\,\bar{\varepsilon}_h^{-1}\,\bar{\delta}^{\,t} S_e k y_e^c 2 \begin{bmatrix} c-\gamma_e & \alpha_e \\ -\alpha_e & \gamma_e \end{bmatrix} \begin{bmatrix} \tilde{\Psi}_{eA} \\ \tilde{\Psi}_{eA} \end{bmatrix} + \sqrt{\varepsilon_{re}}\ S_h \begin{bmatrix} \tilde{\Psi}_{hA} \\ \tilde{\Psi}_{hA} \end{bmatrix} \tag{29}$$

$$\eta_o \begin{bmatrix} \bar{H}_{yA} \\ \bar{H}_{yB} \end{bmatrix} = -\,\bar{\delta}\, S_h k y_h^c 2 \begin{bmatrix} c-\gamma_h & \alpha_h \\ -\alpha_h & \gamma_h \end{bmatrix} \begin{bmatrix} \tilde{\Psi}_{hA} \\ \tilde{\Psi}_{hA} \end{bmatrix} + \sqrt{\varepsilon_{re}}\ S_e \begin{bmatrix} \tilde{\Psi}_{eA} \\ \tilde{\Psi}_{eA} \end{bmatrix} \tag{30}$$

After discarding the potentials $\tilde{\Psi}_e$ and $\tilde{\Psi}_h$ by means of (25) and (26) respectively, one can finally get a relation between tangential components at interfaces A and B as

$$\begin{bmatrix} j\bar{E}_{zA} \\ j\bar{E}_{zB} \end{bmatrix} = -\eta_o\ S_h k y_h^c 2 \begin{bmatrix} c-\gamma_h & \alpha_h \\ -\alpha_h & \gamma_h \end{bmatrix}\ S_h^{-1}\, Q_h^{c-1} \begin{bmatrix} \bar{H}_{xA} \\ \bar{H}_{xB} \end{bmatrix} c + \bar{\varepsilon}_h^{-1}\,\tilde{\delta}^{\,t} Q_e^{c-1} \bar{\varepsilon}_e \begin{bmatrix} \bar{E}_{xA} \\ \bar{E}_{xB} \end{bmatrix} \tag{31}$$

$$\eta_o \begin{bmatrix} j\bar{H}_{zA} \\ j\bar{H}_{zB} \end{bmatrix} = -S_e k y_e^c 2 \begin{bmatrix} c-\gamma_e & \alpha_e \\ -\alpha_e & \gamma_e \end{bmatrix} S_e^{-1}\, Q_e^{c-1} \bar{\varepsilon}_e \begin{bmatrix} \bar{E}_{xA} \\ \bar{E}_{xB} \end{bmatrix} + \eta_o\ \tilde{\delta}\ Q_h^{c-1} \begin{bmatrix} \bar{H}_{xA} \\ \bar{H}_{xB} \end{bmatrix} \tag{32}$$

The field components in y-direction are given by

$$\begin{bmatrix} \bar{E}_{yA} \\ \bar{E}_{yB} \end{bmatrix} = -\,\bar{\varepsilon}_h^{-1}\,\bar{\delta}^{\,t} S_e k y_e^c 2 \begin{bmatrix} c-\gamma_e & \alpha_e \\ -\alpha_e & \gamma_e \end{bmatrix} S_e^{-1}\, Q_e^{c-1} \bar{\varepsilon}_e \begin{bmatrix} \bar{E}_{xA} \\ \bar{E}_{xB} \end{bmatrix} + \eta_o \sqrt{\varepsilon_{re}}\ Q_h^{c-1} \begin{bmatrix} \bar{H}_{xA} \\ \bar{H}_{xB} \end{bmatrix} \tag{33}$$

$$\eta_o \begin{bmatrix} \bar{H}_{yA} \\ \bar{H}_{yB} \end{bmatrix} = -\eta_o \bar{\delta}\ S_h k y_h^c 2 \begin{bmatrix} c-\gamma_h & \alpha_h \\ -\alpha_h & \gamma_h \end{bmatrix}\ S_h^{-1}\, Q_h^{c-1} \begin{bmatrix} \bar{H}_{xA} \\ \bar{H}_{xB} \end{bmatrix} c - \sqrt{\varepsilon_{re}}\, Q_e^{c-1} \bar{\varepsilon}_e \begin{bmatrix} \bar{E}_{xA} \\ \bar{E}_{xB} \end{bmatrix} \tag{34}$$

Using eq. (12), the two systems (31) and (32) are converted to the forms below

$$\eta_o \begin{bmatrix} \bar{H}_{xA} \\ \bar{H}_{xB} \end{bmatrix} = B_h \tilde{\lambda}_h \begin{bmatrix} \gamma_h & \alpha_h \\ \alpha_h & \gamma_h \end{bmatrix} B_h^{-1} \begin{bmatrix} -j\bar{E}_{zA} \\ j\bar{E}_{zB} \end{bmatrix} + B_h \begin{bmatrix} \gamma_h & \alpha_h \\ \alpha_h & \gamma_h \end{bmatrix} \tilde{\lambda}_h B_h^{-1} \bar{\varepsilon}_h^{-1} \tilde{\delta}^t Q_e^{c-1} \bar{\varepsilon}_e \begin{bmatrix} \bar{E}_{xA} \\ -\bar{E}_{xB} \end{bmatrix} \tag{35}$$

$$\eta_o \begin{bmatrix} -j\bar{H}_{xA} \\ -j\bar{H}_{xB} \end{bmatrix} = S_h \tilde{\lambda}_h \begin{bmatrix} \gamma_h & \alpha_h \\ \alpha_h & \gamma_h \end{bmatrix} S_h^{-1} \begin{bmatrix} -j\bar{E}_{zA} \\ j\bar{E}_{zB} \end{bmatrix} - \left(S_e k y_e^c 2 \begin{bmatrix} \gamma_e & \alpha_e \\ \alpha_e & \gamma_e \end{bmatrix} \tilde{\lambda}_e S_e^{-1} Q_e^{c-1} \bar{\varepsilon}_e - \tilde{\delta}\, S_h \begin{bmatrix} \gamma_h & \alpha_h \\ \alpha_h & \gamma_h \end{bmatrix} S_h^{-1} \bar{\varepsilon}_h^{-1} \tilde{\delta}^t Q_e^{c-1} \bar{\varepsilon}_e \right) \begin{bmatrix} \bar{E}_{xA} \\ -\bar{E}_{xB} \end{bmatrix} \tag{36}$$

Using $S^{-1}Q^{-1} = \lambda^{-1}S^{-1}$ derived from (12), one finally obtains for the y-field components as

$$\begin{bmatrix} \bar{E}_{yA} \\ \bar{E}_{yB} \end{bmatrix} = \bar{\varepsilon}_h^{-1} \bar{\delta}^t S_e k y_e^c 2 \begin{bmatrix} \gamma_e & \alpha_e \\ \alpha_e & \gamma_e \end{bmatrix} \tilde{\lambda}_e^{-1} S_e^{-1} \bar{\varepsilon}_e \begin{bmatrix} \bar{E}_{xA} \\ -\bar{E}_{xB} \end{bmatrix} c - \eta_o \sqrt{\varepsilon_{re}}\; Q_h^{c-1} \begin{bmatrix} \bar{H}_{xA} \\ \bar{H}_{xB} \end{bmatrix} \tag{37}$$

$$\eta_o \begin{bmatrix} \bar{H}_{yA} \\ \bar{H}_{yB} \end{bmatrix} = \eta_o \bar{\delta}\, S_h k y_h^c 2 \begin{bmatrix} \gamma_h & \alpha_h \\ \alpha_h & \gamma_h \end{bmatrix} \tilde{\lambda}_h^{-1}\; S_h^{-1} \begin{bmatrix} \bar{H}_{xA} \\ -\bar{H}_{xB} \end{bmatrix} c - \sqrt{\varepsilon_{re}}\, Q_e^{c-1} \bar{\varepsilon}_e \begin{bmatrix} \bar{E}_{xA} \\ \bar{E}_{xB} \end{bmatrix} \tag{38}$$

(35) and (36) can be collated using the definition of the field vector as

$$H_{A,B} = \eta_o \begin{bmatrix} -jH_{zA,B} \\ H_{xA,B} \end{bmatrix} \quad ; \quad E_{A,B} = \begin{bmatrix} E_{xA,B} \\ -jE_{zA,B} \end{bmatrix} \text{ and } \bar{y}_1 = \begin{bmatrix} \tilde{\gamma}_H \rho_e & \tilde{\delta}\, \tilde{\gamma}_h \\ \tilde{\gamma}_h\, \rho & \tilde{\gamma}_E \end{bmatrix}; \bar{y}_2 = \begin{bmatrix} \tilde{\alpha}_H \rho_e & \tilde{\delta}\, \tilde{\alpha}_h \\ \tilde{\alpha}_h\, \rho & \tilde{\alpha}_E \end{bmatrix} \tag{39}$$

in the form

$$\begin{bmatrix} \overline{H_A} \\ \overline{H}_B \end{bmatrix} = \begin{bmatrix} \overline{y}_1 & \overline{y}_2 \\ \overline{y}_2 & \overline{y}_1 \end{bmatrix} \begin{bmatrix} \overline{E_A} \\ -\overline{E}_B \end{bmatrix} \tag{40a}$$

Where the following abbreviations must hold:

$$\tilde{\gamma}_h = S_h \gamma_h S_h^{-1} \quad ;$$

$$\tilde{\alpha}_h = S_h \alpha_h S_h^{-1}$$

$$\tilde{\gamma}_E = S_h \tilde{\lambda}_h \gamma_h S_h^{-1} \quad ; \quad \tilde{\alpha}_E = S_h \tilde{\lambda}_h \alpha_h S_h^{-1}$$

$$\tilde{\gamma}_e = S_e k y_e^c 2 \gamma_e S_e^{-1} \quad ; \quad \tilde{\alpha}_e = S_e k y_e^c 2 \alpha_e S_e^{-1}$$

$$\rho_e = Q_e^{-1} \bar{\varepsilon}_e = \left(\bar{\delta}\, \bar{\varepsilon}_h^{-1}\, \bar{\delta}^t c - I_e \right)^{-1} \quad ; \quad \rho_h = Q_h^{-1} \bar{\varepsilon}_h^{-1} = \bar{\lambda}_h \bar{\varepsilon}_h^{-1} - I_h$$

$$\rho_e = \rho_e\, \tilde{\delta}^t \rho_e \tag{40b}$$

It worth noting that $\overline{y}_1$, $\overline{y}_2$ are not diagonal matrices.

2.3. Matching Equations

The wave equations are solved separately in each region of the considered structure, using appropriate potential functions or directly utilizing the electromagnetic field components, according to homogeneous/inhomogeneous regions as well as isotropic/anisotropic dielectric substrates. It is worth also to note that for all chosen related potential functions, the electromagnetic field components should coincide with each other; This means that each electric field component, say *Ex*, has to be aligned with the same electric field component of its neighborhood regions. Hence a special care needs to be taken during derivation if the boundary conditions change from one region to another. The detailed derivation of the matching field expressions is given in appendix A.

Using the results obtained in appendix A, one can see that in order to represent the tangential electromagnetic field in spatial domain, (A5)–(A9) have to be expressed back into the original domain. The inverse transformations must be performed according to the field subvectors of interest represented by (A10)–(A13).

Collating the subvectors of the field components of the same kind and the same interface i according to

$$E_i = \begin{bmatrix} E_{x_i} \\ -jE_{z_i} \end{bmatrix} \quad ; \quad H_i = \eta_c o \begin{bmatrix} -jH_{z_i} \\ H_{x_i} \end{bmatrix} \tag{41}$$

The tangential electromagnetic field components of the layers I and III in the original domain, after performing the inverse transformation, are given by

$$H_A^I = y_1^I E_A^I \tag{42}$$

and

$$H_D^V = -y_1^V E_D^V \tag{43}$$

However for layers II and IV, the subvector fields relation-ship that are necessary for field matching are given in the spatial domain by

$$\begin{bmatrix} H_A^I \\ H_B^{III} \end{bmatrix} = \begin{bmatrix} M_{11}^{II} & M_{12}^{II} \\ M_{21}^{II} & M_{22}^{II} \end{bmatrix} \begin{bmatrix} E_A^I \\ -E_B^{III} \end{bmatrix} \tag{44}$$

for layer II, and for layer IV they are given by:

$$\begin{bmatrix} H_C^{III} \\ H_D^V \end{bmatrix} = \begin{bmatrix} M_{11}^{IV} & M_{12}^{IV} \\ M_{21}^{IV} & M_{22}^{IV} \end{bmatrix} \begin{bmatrix} E_C^{III} \\ -E_D^V \end{bmatrix} \tag{45}$$

In equations (44) and (48) $M_{ij}^{II,IV}$ $\{ i,j = 1,2 \}$ are the reduced matrices obtained by inverse transformation, which are of appropriate size following the corresponding dimensions of the tangential field components of the field vectors E and H at each metallization interface.

From (41)–(48) the following matching field equations might be elaborated

$$y_1^I E_A^I = M_{11}^{II} E_A^I - M_{12}^{II} E_B^{III} \tag{46a}$$

$$c{-}y_1^V E_D^V = M_{21}^{IV} E_C^{III} - M_{22}^{IV} E_D^V \tag{46b}$$

$$y_1^{III} E_B^{III} - y_2^{III} E_C^{III} = M_{21}^{II} E_A^I - M_{22}^{II} E_B^{III} \tag{46c}$$

$$y_2^{III} E_B^{III} - y_1^{III} E_C^{III} = M_{11}^{IV} E_C^{III} - M_{12}^{IV} E_D^V \tag{46d}$$

Form (**??**), the field E_c can be expressed in terms of E_B^{III} and E_A^I as

$$E_C^{III} = -M_{CA} E_A^I + M_{CB} E_B^{III} \tag{47}$$

where

$$M_{CA}c = \left(y_2^{III}\right)^{-1} M_{21}^{II} \quad M_{CB} = \left(y_2^{III}\right)^{-1} \left(y_1^{III} + M_{22}^{II}\right)$$

It is important to note that the inversion of y_2^{III} can be performed analytically.

Substituting E_C^{III} given by (47) into (46a)–(46c), the following eigenvalue system (ε_{eff} as eigenvalue) is achieved. Thus

$$\begin{bmatrix} M_{11}^{II}c - y_1^I & M_{12}^{II} & 0 \\ M_{21}^{IV} M_{CA} & M_{21}^{IV} M_{CB} & M_{22}^{IV}c - y_1^V \\ \left(y_1^{III} + M_{11}^{IV}\right) M_{CA} & \left(y_1^{III} + M_{11}^{IV}\right) M_{CB} - y_2^{III} & M_{12}^{IV} \end{bmatrix} \begin{bmatrix} E_A^I \\ -E_B^{III} \\ E_D^V \end{bmatrix} = 0 \tag{48}$$

or in a simpler form as

$$[M_{red}(\varepsilon_{eff})] \begin{bmatrix} E_A^I \\ -E_B^{III} \\ E_D^V \end{bmatrix} = 0 \tag{49}$$

This system (49) possesses a non trivial solution if its determinant vanishes

$$\det\left\{[M_{red}(\varepsilon_{eff})]\right\} = 0 \tag{50}$$

3. Results and Discussion

To demonstrate the computational efficiency of the technique used, a performance analysis has been done for a unilateral finline structure as it is the targeted structure. The results are embodied in Appendix B below.

The influence of substrate mounting groove depth wg on the normalized propagation constant and characteristic impedance is demonstrated for both unilateral and bilateral finline structures centered in the waveguide housing. Figure 4 shows the normalized propagation constant ε_{eff} of the dominant and First higher order odd mode for the groove depths of $wg/d = 0$ and $wg/d \neq 0$ (Figure 4-a and Figure 4-b) with a metallization thickness of $t/d = 0.045$. The trend of our results show consistency with those published in [11] employing the conservation of complex power technique.

In these figures, it is observed that when the mounting groove depth is taken into account, the propagation constant increases while the cut-off frequency is decreases with respect. These changes are mainly due to the presence of a part of dielectric slab within the mounting groove depth wg. It can be clearly noticed that, when the first higher mode starts to propagate, the dominant mode is considerably affected. Moreover, the cut-off frequency of the first higher order mode, which limits the most interesting monomode range in practical situations, is largely reduced, unlike the one of the dominant mode indicated in [11]. Note also the reduction of the bandwidth that results from consideration of the mounting grooves.

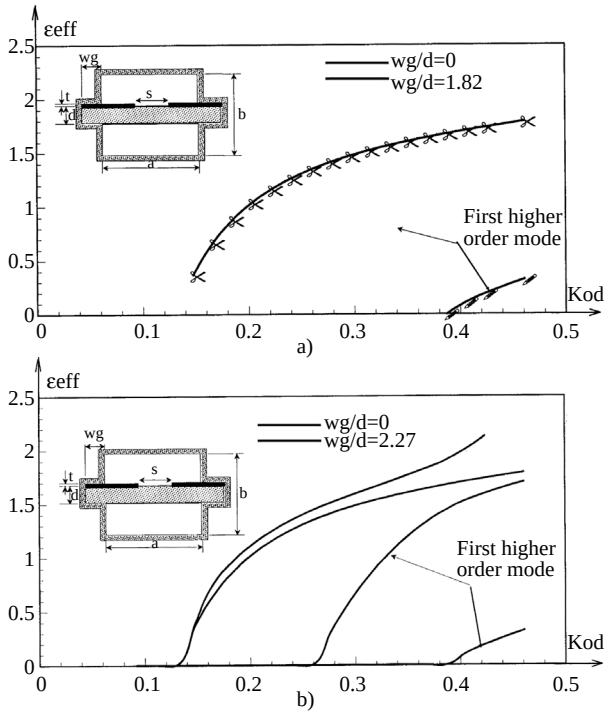

Figure 4. Hybrid-mode and higher order mode versus normalized frequency in unilateral finline structure with a/d = 7.5, b/d = 15, s/d = 2.72, t/d = 0.045, (a): wg/d = 1.82; (b): wg/d = 2.27.

The effect of mounting groove depth *wg* on the characteristic impedance *Zc* for the unilateral finline is illustrated in Figure 5. As it has been pointed out earlier, the trend of the computed results are consistent with those published in [11] even though these last ones are plotted as a function of frequency. It can be observed from Figure 5 that the deviations of the characteristic impedance from the ideal case where *wg* = 0 become more significant as the first higher order mode starts propagating.

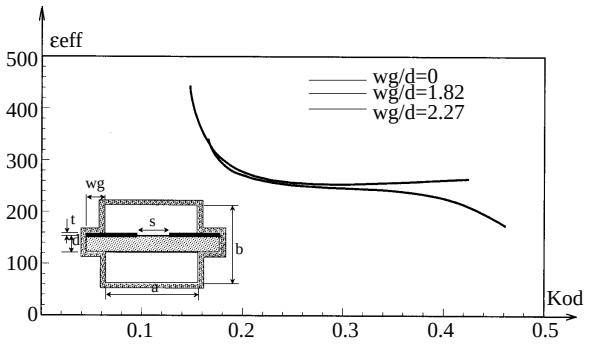

Figure 5. Characteristic impedance versus normalized frequency in unilateral finline structure with a/d = 7.5,b/d = 15, s/d = 2.72, t/d = 0.045; for different grooves' depths: wg/d = 0; wg/d = 1.82; wg/d = 2.27.

Figures 6 a), b) and c) show the effect of the groove depth *wg* on the propagation constant ε_{eff} versus normalized frequency d/λo for a bilateral finline structure with fixed finite metallization thickness $t = 0.04$.

In this case the different grooves' depths have values *wg/d = 1.6* (Figure 6-a), *wg/d = 4.8* (Figure

6-b) and $wg/d = 8$ (Figure 6-c). Note that both the hybrid mode and the first higher mode are not seriously affected when the mounting grooves are taken into account.

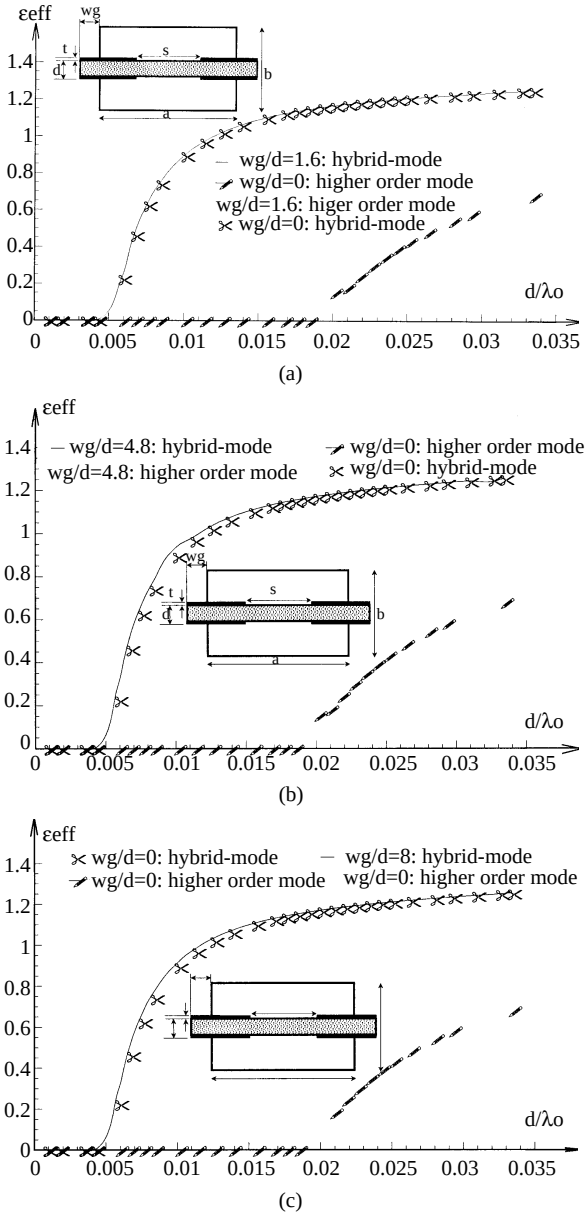

Figure 6. Hybrid-mode and higher modes dispersion characteristics versus normalized frequency of bilateral finline structure for various groove depths with: a/d = 56.9, b/d = 28.45, s/d = 2.72, t/d = 0.04, εr = 3; and different groove depths: (a) - wg/d = 1.6; (b), - wg/d = 4.8; (c) - wg/d = 8.

Also shown in Figure 7, is the characteristic impedance versus normalized frequency d/λo for different values of groove depths. Note the slight change of the characteristic impedance when the groove depths are considered.

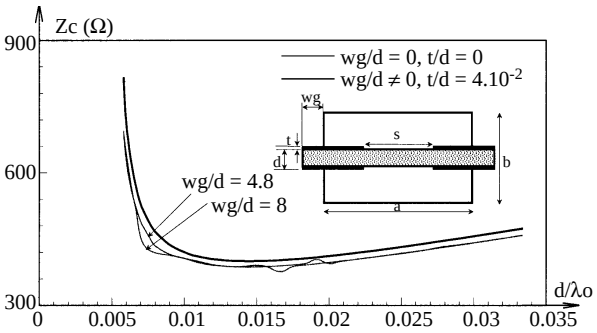

Figure 7. Characteristic impedance versus normalized frequency for bilateral finline structure for various grooves' depths with: a/d = 56.9, b/d = 28.45, s/d = 2.72, t/d = 0.04, εr = 3; and different groove depths: wg/d = 0; wg/d = 4.8; wg/d = 8.

For practical applications, when the unilateral finline structure is used along with active components, one or both fins are insulated by a gasket which allows a dc voltage to be developed across them.

The dispersion curves of the propagation constant for the so called "isolated finline" are presented in Figure 8. It This figure shows the effect of various gasket heights gh/d on frequency dependent dominant mode of isolated unilateral finline structure for different mounting groove depths wg/d and fixed metallization thickness t/d (assuming $\varepsilon_r = 1$ for the gasket insulation dielectric layer) e. It is also observed that, dispersion

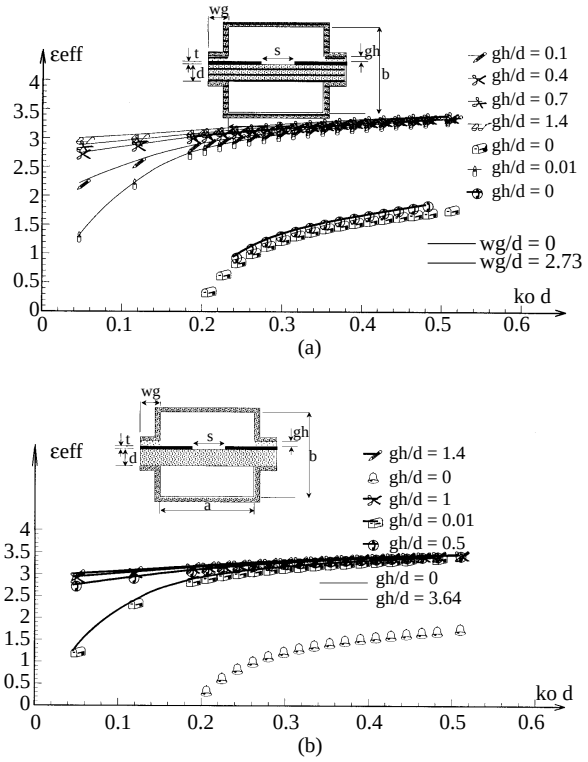

Figure 8. Effect of gasket insulator on the dispersion dielectric constant εeff for fixed metallization thickness and various goove depths of unilateral finline structure with a/d = 6.82, b/d = 14.1, s/d = 1.82 t/d = 0.023, εr = 3.75,(a): wg/d = 2.72, - (b): wg/d = 3.64.

characteristics ε_{eff} versus normalized frequency $d/\lambda o$ is greatly affected when the insulation gasket is used. This effect becomes more pronounced as the insulation gasket height increases. Moreover, the effective dielectric constant has no cut-off frequency when insulation gasket is used since the dominant mode propagating at low frequencies is Quasi-TEM.

However, the dispersion characteristics of the effective dielectric constant ε_{eff} versus normalized frequency d/λo is greatly affected when dielectric gasket is used.

Figure 9 illustrates the effect of using an insulating gasket in a finline structure on the characteristic impedance Z_c. The impedance follows the same behavior as of the effective dielectric constant which is characterized by low values at low frequencies because the dominant propagating mode is a quasi-TEM. For higher frequencies, however, the impedance becomes higher and closer to that of an ideal structure. This can be explained by the fact that beyond a certain range of frequencies, the strip conductor becomes short-circuited to the metallic housing and, hence, behaves as an ideal finline structure.

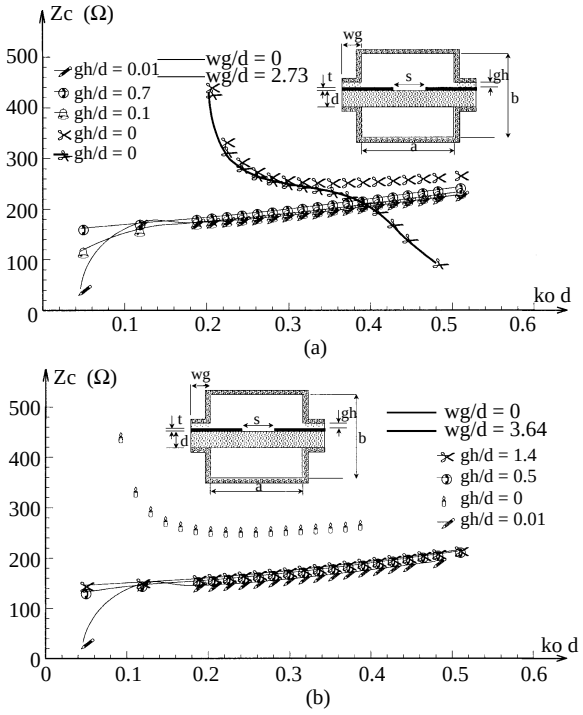

Figure 9. Effect of gasket insulator on the characteristic impedance Zc with fixed metallization thickness and various groove depths of unilateral finline structure with a/d = 6.82, b/d = 14.1, s/d = 1.82, t/d = 0.023, εr = 3.75, - (a): wg/d = 2.72, - (b): wg/d = 3.64.

4. Conclusion

Mathematical derivations and numerical computations based on the method of Lines presented in this paper provide a further confirmation of the validity of the technique used and show its simplicity for treating different types of planar structures. The characterization of finline structures with complex configurations corresponding to real situations are of particular interest and their analysis can easily be extended to characterize other E-plane transmission structures of similar architectures.

The unilateral and bilateral finline structures including most of their practical parameters, such as metallization thickness and grooves' depths, have been also investigated. The effect of these realistic parameters have been discussed and the results show that, at higher frequencies, the grooves supporting the substrate cannot be neglected and, in addition, their influence is more significant than the effect of finite metallization thickness. Other unilateral finline structure, known as the "isolated finline" with more complex configuration required in practical applications with active components, was also analyzed. This real structure supports TEM mode and does not have a cut-off frequency as the ideal finline structure. The derived results confirm some of the practical outcomes predicted in the literature.

Appendix A: Derivation of Field matching equations

Note that for a region having a certain thickness, a relationship between the transformed electromagnetic field components, that are necessary for the matching on the interfaces, can be established. That is for a region which has a top and bottom interfaces denoted respectively by $(+)$ and $(-)$, this relation can be written in a shorter way as

$$\begin{bmatrix} \bar{H}_- \\ \bar{H}_+ \end{bmatrix} = \begin{bmatrix} \overline{y}_1^R & \overline{y}_2^R \\ \overline{y}_2^R & \overline{y}_1^R \end{bmatrix} \begin{bmatrix} \bar{E}_- \\ \bar{E}_+ \end{bmatrix} \qquad (A1)$$

Where $\overline{y}_k^R \ \{k = 1, 2\}$ are summarized hereafter for each region properties. For an isotropic homogeneous region, it is given by

$$\overline{y}_1^R = \begin{bmatrix} -\varepsilon_d \gamma_h & \gamma_h \tilde{\delta} \\ \tilde{\delta}^t \gamma_h & \gamma_E \end{bmatrix}_R \quad ; \quad \overline{y}_2^R = \begin{bmatrix} -\varepsilon_d \alpha_h & \alpha_h \tilde{\delta} \\ \tilde{\delta}^t \alpha_h & \alpha_E \end{bmatrix}_R \qquad (A2-a)$$

with

$$\tilde{\delta} = \sqrt{\varepsilon_{re}\overline{\delta}} \quad ; \quad \begin{Bmatrix} \alpha_E \\ \gamma_E \end{Bmatrix} = (\overline{\lambda}_e - \varepsilon_r) \begin{Bmatrix} \alpha_e \\ \gamma_e \end{Bmatrix} \qquad (A2-b)$$

On the other hand, for the uniaxial anisotropic substrate with homogeneous region, this relation becomes

$$\overline{y}_1 = \begin{bmatrix} -\tilde{\gamma}_H & \tilde{\delta}\,\bar{\gamma}_e + \tilde{\gamma}_h \tilde{\delta} \\ \bar{\gamma}_e \tilde{\delta}^t + \tilde{\delta}^t \tilde{\gamma}_h & \tilde{\gamma}_E \end{bmatrix} \quad ; \quad \overline{y}_2 = \begin{bmatrix} -\tilde{\alpha}_H & \tilde{\delta}\,\bar{\alpha}_e + \bar{\alpha}_h \tilde{\delta} \\ \bar{\alpha}_e \tilde{\delta}^t + \tilde{\delta}^t \bar{\alpha}_h & \tilde{\alpha}_E \end{bmatrix} \qquad (A3-a)$$

with

$$\begin{aligned} &\bar{\alpha}_e = \varepsilon_\perp (\overline{\lambda}_e + \varepsilon_{re} I)^{-1} \alpha_e ; \tilde{\alpha}_E = \overline{\delta}^t \bar{\alpha}_h \overline{\delta} - \varepsilon_{re} \bar{\alpha}_e \\ &\bar{\gamma}_e = \varepsilon_\perp (\overline{\lambda}_e + \varepsilon_{re} I)^{-1} \gamma_e ; \tilde{\gamma}_E = \overline{\delta}^t \tilde{\gamma}_h \overline{\delta} - \varepsilon_{re} \bar{\gamma} \\ &\bar{\alpha}_h = k_{y_h}^2 \alpha_h (\overline{\lambda}_h + \varepsilon_{re} I)^{-1} c ; \tilde{\alpha}_H = \overline{\delta}\,\bar{\alpha}_e \overline{\delta}^t - \varepsilon_{re} \bar{\alpha}_h \\ &\bar{\gamma}_h = k_{y_h}^2 \gamma_h (\overline{\lambda}_h + \varepsilon_{re} I)^{-1} c ; \tilde{\gamma}_H = \overline{\delta} \bar{\gamma}_e \overline{\delta}^t - \varepsilon_{re} \tilde{\gamma}_h \end{aligned} \qquad (A3-b)$$

For an isotropic inhomogeneous layer, it is given by

$$\bar{y}_1 = \begin{bmatrix} \tilde{\gamma}_H \rho_e & \tilde{\delta}\,\tilde{\gamma}_h \\ \tilde{\gamma}_h\ \rho & \tilde{\gamma}_E \end{bmatrix} \quad ; \quad \bar{y}_2 = \begin{bmatrix} \tilde{\alpha}_H \rho_e & \tilde{\delta}\,\tilde{\alpha}_h \\ \tilde{\alpha}_h\ \rho & \tilde{\alpha}_E \end{bmatrix} \qquad (A4)$$

Generally, the matrices λ, ky, α, γ, δ and T are inherent to each region and depend upon the number of discretization lines in each region and the associated boundaries.

The relationship between the transformed tangential field components at the interfaces A is given by

$$\begin{bmatrix} -j\overline{H}^I_{xA} \\ \overline{H}^I_{zA} \end{bmatrix} = - \begin{bmatrix} \overline{y}^I_{11} & \overline{y}^I_{12} \\ \overline{y}^I_{21} & \overline{y}^I_{22} \end{bmatrix} \begin{bmatrix} \overline{E}^I_{xA} \\ -j\overline{E}^I_{zA} \end{bmatrix} \qquad (A5-a)$$

or in a shorter form as

$$\overline{H}^I_A = -\overline{y}^I_1 \overline{E}^I_A \qquad (A5-b)$$

and for the region V at the interface D, the established relation can be written as

$$\begin{bmatrix} -j\overline{H}^V_{xD} \\ \overline{H}^V_{zD} \end{bmatrix} = \begin{bmatrix} \overline{y}^V_{11} & \overline{y}^V_{12} \\ \overline{y}^V_{21} & \overline{y}^V_{22} \end{bmatrix} \begin{bmatrix} \overline{E}^V_{xD} \\ -j\overline{E}^V_{zD} \end{bmatrix} \qquad (A6-a)$$

Or can be expressed in a more compacted form as

$$\overline{H}^V_D = \overline{y}^V_1 \overline{E}^V_D \qquad (A6-b)$$

For the inhomogeneous region IV with two interfaces C and D, the connection of the tangential electromagnetic field components at these interfaces are related with the following reduced expression:

$$\begin{bmatrix} \overline{H}^{IV}_C \\ \overline{H}^{IV}_D \end{bmatrix} = \begin{bmatrix} \overline{y}^{IV}_1 & \overline{y}^{IV}_2 \\ \overline{y}^{IV}_2 & \overline{y}^{IV}_1 \end{bmatrix} \begin{bmatrix} \overline{E}^{IV}_C \\ -\overline{E}^{IV}_D \end{bmatrix} \qquad (A7)$$

Note also that the regions II and III have also two interfaces each, which are B-C and A-B.

The relationship of the tangential field components for these two regions at their corresponding interfaces are given by

$$\begin{bmatrix} \overline{H}^{II}_A \\ \overline{H}^{II}_B \end{bmatrix} = \begin{bmatrix} \overline{y}^{II}_1 & \overline{y}^{II}_2 \\ \overline{y}^{II}_2 & \overline{y}^{II}_1 \end{bmatrix} \begin{bmatrix} \overline{E}^{II}_A \\ -\overline{E}^{II}_B \end{bmatrix} \qquad (A8)$$

$$\begin{bmatrix} \overline{H}^{III}_B \\ \overline{H}^{III}_C \end{bmatrix} = \begin{bmatrix} \overline{y}^{III}_1 & \overline{y}^{III}_2 \\ \overline{y}^{III}_2 & \overline{y}^{III}_1 \end{bmatrix} \begin{bmatrix} \overline{E}^{III}_B \\ -\overline{E}^{III}_C \end{bmatrix} \qquad (A9)$$

The field matching at interfaces A, B, C and D have to be done in spatial domain.

At the interfaces A and D, one can have

$$\overline{E}^{II}_{xA} = \begin{bmatrix} 0 \\ E^I_{xA} \\ 0 \end{bmatrix} \quad , \quad \overline{E}^{II}_{zA} = \begin{bmatrix} 0 \\ E^I_{zA} \\ 0 \end{bmatrix} \quad , \quad \overline{H}^{II}_{xA} = \begin{bmatrix} H^{II}_{xAM1} \\ H^I_{xA} \\ H^{II}_{xAM2} \end{bmatrix} \quad , \quad \overline{H}^{II}_{zA} = \begin{bmatrix} H^{II}_{zAM1} \\ H^I_{zA} \\ H^{II}_{zAM2} \end{bmatrix} \qquad (A10)$$

$$\overline{E}^{IV}_{xD} = \begin{bmatrix} 0 \\ E^V_{xD} \\ 0 \end{bmatrix} \quad , \quad \overline{E}^{IV}_{zD} = \begin{bmatrix} 0 \\ E^V_{zD} \\ 0 \end{bmatrix} \quad , \quad \overline{H}^{IV}_{xD} = \begin{bmatrix} H^{IV}_{xDM1} \\ H^V_{xD} \\ H^{IV}_{xAM2} \end{bmatrix} \quad , \quad \overline{H}^{IV}_{zD} = \begin{bmatrix} H^{IV}_{zDM1} \\ H^I_{zD} \\ H^{II}_{zAM2} \end{bmatrix} \qquad (A11)$$

Where M1 and M2 are subscripts used in the field components to describe the metallization component parts lying along the groove depth. However for the interfaces B and C, the component of interest are given by the following expression

$$\overline{E}^{II}_{xB} = \begin{bmatrix} 0 \\ E^{III}_{xB} \\ 0 \end{bmatrix} \quad , \quad \overline{E}^{II}_{zB} = \begin{bmatrix} 0 \\ E^{III}_{zB} \\ 0 \end{bmatrix} \quad , \quad \overline{H}^{II}_{xB} = \begin{bmatrix} J^1_{zB} \\ H^{III}_{xB} \\ J^2_{zB} \end{bmatrix} \quad , \quad \overline{H}^{II}_{zB} = \begin{bmatrix} -J^1_{xB} \\ H^{III}_{zB} \\ -J^2_{xB} \end{bmatrix} \qquad (A12)$$

$$^{II}_{xC} = \begin{bmatrix} 0 \\ E^{III}_{xC} \\ 0 \end{bmatrix} \quad , \quad \overline{E}^{II}_{zC} = \begin{bmatrix} 0 \\ E^{III}_{zC} \\ 0 \end{bmatrix} \quad , \quad \overline{H}^{II}_{xC} = \begin{bmatrix} -J^1_{zC} \\ H^{III}_{xC} \\ -J^2_{zC} \end{bmatrix} \quad , \quad \overline{H}^{II}_{zB} = \begin{bmatrix} J^1_{xC} \\ H^{III}_{zC} \\ -J^2_{xC} \end{bmatrix} \qquad (A13)$$

In the last two equations (A12) and (A13) the superscript in the current J indicates the 1^{st} and 2^{nd} conductor at the metallization interface.

Appendix B: Performance of the computational approach

Among the well known advantages of the MoL, are its reduced discretization error, relatively simple to formulate and has got an optimal edge positioning scheme which contribute to reduction in computing time. In fact, discretization line positioning is very important for convergence of the solution, as it is the main parameter in defining the rate of convergence. This is unlike other methods, such as the Mode Matching Technique (MMT), where the solution may converge towards a wrong value. This happens for the MMT if the edge condition of the metallic strips is violated.

On the contrary, the convergence using the Method of Lines is always assured. However, at the vicinity of the strip edges, where field singularities occur, large discretization errors may arise. To minimize these errors, an optimal edge positioning criteria at the metallic edges needs to be examined [18].

The draw back of the method of lines appears in very unfamiliar cases where there is extreme difference in the width of metallic strip conductors or gaps between strips. In this case, the total number of discretization needs to be considerably increased to maintain good accuracy. This affects mainly the memory space and computing time requirements. However, the number of required lines can be reduced using a non uniform discretization scheme as has been done in this work.

In the present work, the performance of the described method has been verified for unilateral finline structure with finite metallization thickness. The numerical results for the dielectric constant ε_{eff} and the characteristic impedance *Zc* are shown in Figure 10 These curves are represented as function of normalized discretization width *(a/d)/(n+1) = h/d* (n is the total number of discretization lines), for $d/\lambda o = 0.0102$ and $d/\lambda o = 0.0296$. It appears from these figures that, if the discretization width decreases towards zero, the calculated ε_{eff} and *Zc* always converge. As a result, an extrapolation to the exact value is possible.

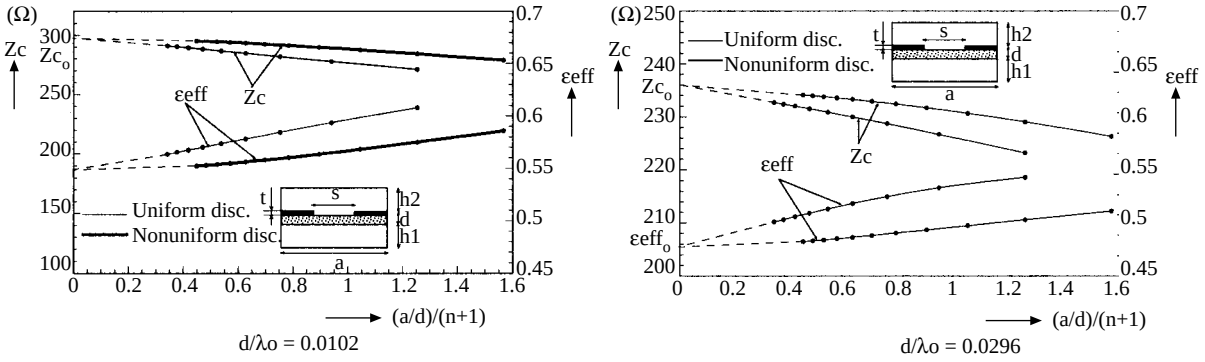

Figure 10. Convergence behavior of ε_{eff} and Zc for unilateral finline structure using the uniform and nonuniform discretization as function of (a/d)/(n+1).a/d = 18.8,h1/d = 18.8, h2/d = 17.8, s/d = 3.76, t/d = 0.79, εr = 3.8.

References

[1] M.V. Schneider, "Microstrip lines for microwave integrated circuits," Bell syst. Tech. J., Vol. 48, pp. 1421-1444, 1969.

[2] P.J. Meier, "Integrated finline millimeter components," IEEE trans. Microwave theory and Tech., Vol. MTT-22, pp. 1209-1216, Dec. 1974

[3] L.P. Schmidt, T. Itoh, "Spectral domain analysis of dominant and higher order modes in finlines," IEEE trans. Microwave theory and Tech., Vol. MTT-28, pp. 981-985, Sept. 1980.

[4] L.P. Schmidt, T. Itoh, H. Hofmann, "Characteristics of unilateral finline structures with arbitrarily located slots," IEEE trans. Microwave theory and Tech., Vol. MTT-29, pp. 352-355, 1981.

[5] A.K. Saad, K. Schunemann, "Efficient eigenmode analysis for planar transmission lines," IEEE trans. Microwave theory and Tech., Vol. MTT-30, pp. 2125-2132, Dec. 1982.

[6] A.K. Saad, K. Schunemann, "A simple method for analyzing fin-line structure," IEEE trans. Microwave theory and Tech., Vol. MTT-26, pp. 1002-1007, Dec. 1978.

[7] B.M. Sherill, N. Alexopoulos, "The method of lines applied to a finline/strip configuration on an anisotropic substrate," IEEE trans. Microwave theory and Tech., Vol. MTT-35, pp. 568-575, 1987.

[8] A. Bayer, "Analysis of the characteristics of an earthed finline," IEEE trans. Microwave theory and Tech., Vol. MTT-29, pp. 676-680, Jul. 1981.

[9] R. Vahldieck, "Accurate hybrid-mode analysis of various finline configurations including multilayered dielectric's, finite metallization thickness, and substrate holding grooves," IEEE trans. Microwave theory and Tech., Vol. MTT-32, pp. 1454-1460, Nov. 1984.

[10] T. Kitazawa, R. Mittra, "Analysis of finline with finite metallization thickness," IEEE trans. Microwave theory and Tech., Vol. MTT-32, pp. 1484-1487, Nov. 1984.

[11] R. R. Mansour, R. H. Macphie, "A unified hybrid-mode analysis for planar transmission line with multilayer isotropic/anisotropic substrates," IEEE trans. Microwave theory and Tech., Vol. MTT-35, pp. 1382-1391, Dec. 1987.

[12] R. Pregla, F. J. Schmückle, "The method of lines for the analysis of planar waveguide structures with finite metallization thickness," (in German), kleinheubacher Ber., Vol.31, pp. 431-438, 1988.

[13] T. Kitazawa, "Metallization thickness effect of striplines with anisotropic media: quasi-static and hybrid-mode analysis," IEEE trans. Microwave theory and Tech., Vol. MTT-35, pp. 769-775, April 1989.

[14] C.J. Railton, J. Mc Geehan, "An analysis of microstrip with rectangular and trapezoidal conductor cross-section," IEEE trans. Microwave theory and Tech., Vol. MTT-38, pp. 1017-1022, Aug. 1990.

[15] J. Gerdes, K. Heiz Helf, R. Pregla, "Full-wave analysis of travelling-wave electrodes with finite thickness for electro-optic modulators by the method of lines," Journal of light Tech., Vol. 9, pp. 461-467, April 1991.

[16] R.E. Collin, Field Theory of Guided Waves, pp. 224-234, Mc Graw-Hill, New-York, 1960.

[17] U. Rogge, R. Pregla, "Method of lines for the analysis of dielectric waveguides", Journal of light Tech., Vol. 11, no 12, pp 2015 – 2020, Dec. 1993

[18] R. Pregla, W. Pasher, "The method of lines" in Numerical Techniques for Microwave and Millimeter wave Passif Structures, T. Itoh, Ed. New-York: Wiley, pp. 381-446, 1989.

[19] L. Yan,; W. Hong,; K. Wu,; T.J. Cui, "Investigations on the propagation characteristics of the substrate integrated waveguide based on the method of lines", Microwaves, Antennas and Propagation, IEE Proceedings –Vol. 152, 1, pp. 35 – 42, Feb. 2005

[20] W. Pascher,; R. Pregla,; L. Vietzorreck, "Fast Full-Wave Analysis of Distributed MEMS Transmission Lines by the MoL", International Conference on Wireless Communications and Applied Computational Electromagnetics, pp. 763 – 766, IEEE/ACES 3-7 April 2005,

[21] A. Ouadi, "Hybrid-mode Analysis of Microwave and Millimeter-wave Structures of Realistic Configurations", Magister thesis, Inelec, Boumerdes, 1995, 03/95.